International Journal of Automotive Technology, Vol. 16, No. 5, pp. 877−883 (2015)
DOI 10.1007/s12239−015−0089−z

pISSN 1229−9138/ eISSN 1976−3832

QUASI-DIMENSIONAL ANALYSIS OF COMBUSTION, EMISSIONS AND KNOCKING IN A HOMOGENEOUS GDI ENGINE

J. LEE[1)], Y. LEE[2)], K. Y. HUH[1)*], H. KWON[2)] and J. I. PARK[3)]

[1)]Department of Mechanical Engineering, Pohang University of Science and Technology, Gyeongbuk 790-784, Korea
[2)]Thermochemical Energy System R&BD Group, Korea Institute of Industrial Technology, 89 Yangdaegiro-gil, Ipjang-myeon, Cheonan-si, Chugnam 331-822, Korea
[3)]Powertrain Thermo-Fluid CAE Team, Hyunadi Motor Group, 150 Hyundaeyeonguso-ro, Hwaseong-si, Gyeonggi 445-709, Korea

(Received 19 May 2014; Revised 6 March 2015; Accepted 8 March 2015)

ABSTRACT− A quasi-dimensional model is developed with the surrogate mechanism of isooctane and n-heptane to predict knock and emissions of a homogeneous GDI engine. It is composed of unburned and burned zone with the latter divided into multiple zones of equal mass to resolve temperature stratification. Combustion is based on turbulent entrainment and burning in a spherically propagating flame with the entrainment rate interpolated between laminar and turbulent flame speed. Validation is performed against measured pressure traces, NOx and CO emissions at different load and rpm conditions. Comparison is made between predictions by the empirical knock model and the chemistry model in this work. There is good agreement for pressure, NOx, CO and knock for the test engine. Promising results are obtained through parametric study with respect to octane number and engine load by the chemistry knock model.

KEY WORDS : Homogeneous GDI, Quasi-dimensional model, Knock, NOx, CO

NOMENCLATURE

A : constant for turbulent burning velocity
C_p : specific heat
D : diffusivity
d_{32} : SMD
h_f : enthalpy of formation
$P_{v,surf}$: saturation pressure
Q_{chem} : heat relrease by knock
Q_{fg} : heat transfer for evaporation
Q_w : heat transfer on the wall
R_v : gas constant
S_L : laminar flame speed
S_T : turbulent burning velocity
V_e : flame propagation speed
z_i : correction factor
α : constant for heat transfer
α, n : constant for flame propagation speed
λ : thermal conductivity, latent heat of evaporation
θ : ignintion delay

SUBSCRIPTS
b : burnd gas
f : fuel
g : gas
i : i-th spray zone
l : liquid
v : vapor

*Corresponding author. e-mail: huh@postech.ac.kr

1. INTRODUCTION

Recently GDI (Gasoline Direct Injection) engines have been popular due to their improved efficiency and emission characteristics in passenger vehicles. An efficient combustion model for GDI engines has become an issue since fuel economy, emission and their accurate predictions are of critical importance to engine developers. We can obtain detailed information from multi-dimensional simulation of combustion processes, although with large computational load involved. There have been recent efforts to develop 0D, 1D and quasi-dimensional codes with advanced physical models for repetitive application in many operating conditions in an engine map. Quasi-dimensional cycle simulation was initially performed with a turbulent flame entrainment model by Blizard and Keck (1974) and later extended by Tabaczynsi *et al.* (1977). The rate of entrainment was assumed proportional to density of unburned gas, entrainment velocity and flame front area (Poulos, 1982). Simulated an SI engine by a quasi-dimensional model with a spherically propagating flame separating burned and unburned zone in an arbitrary chamber shape. NO was calculated in the adiabatic core and the thermal boundary layer by the extended Zel'dovich mechanism under equilibrium assumption for heat release (Han, 1997). Applied turbulence and

combustion models to incorporate the effect of mixing of dilution gas, strong tumble and stratification with substantial EGR (Exhaust Gas Recirculation) in the quasi-dimensional code. The 3D CFM (Coherent Flame Model) was reduced to a simpler version of CFM1D to simulate heat release, knock and pollutants in an SI engine (Malbec *et al.*, 2009). The flame wrinkling factor was estimated from a 0D turbulence model and equilibrium assumption to determine the flame surface density. Detailed chemistry was integrated in the CFM1D to account for the fuel properties of methane-air-diluent mixture (Bougrine *et al.*, 2011). It was based on a priori simulation of 1D premixed flame to generate the chemical data base of composition, laminar flame speed and thickness, which can directly be plugged in the combustion model (Tinaut *et al.*, 1999). Proposed a model based on chemical kinetics to determine CO and NOx and the HC model based on retention in crevices, wall quenching and post-flame combustion processes in the cylinder and exhaust pipe (Grill *et al.*, 2006). Developed a quasi-dimensional model for SI combustion with variable valve timing. This model was able to compute the complete engine map in advance and could rapidly be calibrated. There have been recent studies for quasi-dimensional simulation of GDI engines (D'Errico and Onorati, 2004). Performed integrated simulation of a GDI engine by a quasi-dimensional multi-zone model with the fractal combustion model and with fuel spray divided into fixed zones and burnt gas into zones of equal mass to account for temperature stratification (Schmid *et al.*, 2009). Defined four unburned zones of rich, stoichiometric and lean zones and the remaining air zone for stratified charge in SI engines. These zones were connected to each other by the mass flow rates which were calculated by a mixture model. The new in-cylinder turbulence model was proposed to take into account the interaction of fuel spray and in-cylinder flow for mixture formation (Watanabe, 2010). Predicted turbulence kinetic energy showed good agreement with 3D CFD results, while the burned fuel mass fraction was assumed to follow the Wiebe function with no proper physical consideration (Gong and Rutland, 2013). Developed a quasi-dimensional NOx emission model for GDI engines. The extended Zel'dovich mechanism and the N_2O pathway were employed as the chemical mechanism.

Here we developed a new efficient quasi-dimensional code based on surrogate fuel chemistry for consistent prediction of emissions and knock for different fuels, engine design parameters and operating conditions without arbitrary tuning of model constants. It is applied for calibration of a four stroke cycle homogeneous GDI engine later to be combined with 1D analysis of the entire engine intake and exhaust system. The code includes models for evaporation, burning rate and surrogate mechanisms of iso-octane and n-heptane which are combined with CHEMKIN routines to perform integration of elementary reaction steps together with multi-zone mass and energy conservation equations to consider temperature stratification.

2. GOVERNING EQUATIONS AND SUBMODELS

2.1. Energy Equation

The processes in a GDI engine occur in a continuous sequence of intake, compression, combustion and exhaust strokes. Pressure and turbulent kinetic energy are assumed spatially uniform with fuel/air mixture as homogeneous charge in the cylinder. With early injection a homogeneous GDI engine goes through spark ignition and turbulent premixed flame propagation as in PFI (Port Fuel Injection) engines. The charge composition is characterized by a single mean temperature and assumed frozen during intake, compression and exhaust strokes. During combustion the cylinder charge is divided into unburned zone and burned zone, the latter of which is divided into n zones of equal mass to account for temperature stratification. Each zone has uniform temperature and composition. The energy equation in each zone is described for an open system as,

$$\frac{d(mh)}{dt} - \frac{d(PV)}{dt} = \frac{dQ}{dt} - \frac{dW}{dt} + \sum_{in,out} h_j \frac{dm_j}{dt} \tag{1}$$

where m and V are mass of mixture and volume of cylinder. h is enthalpy, P is pressure and W is work done by the system. The last term represents enthalpy flows through inlet, outlet and fuel injection. Q is the sum of convective heat transfer on the wall, $\dot{Q}_w$, heat transfer to liquid droplets for evaporation, $\dot{Q}_{fg}$, and heat release by decomposition of fuel and knock in the unburned zone, $\dot{Q}_{chem}$, so that $\dot{Q} = -\dot{Q}_w - \dot{Q}_{fg} + \dot{Q}_{chem}$. Convection on chamber wall is the dominant heat transfer mode in SI engines. Radiative heat transfer and heat loss in the exhaust port are neglect in this study. Convective heat transfer on the wall, $\dot{Q}_w$, can be expressed as

$$\dot{Q}_w = hA(T_g - T_w) \tag{2}$$

where h is convective heat transfer coefficient, A is surface area, T_g and T_w are temperatures of gas and wall. h is calculated by the following empirical correlation among

$$Nu = \alpha \mathrm{Re}^{0.8}\mathrm{Pr}^{0.33} = hL/\lambda \tag{3}$$

Nusselt number, Nu, Reynolds number, Re, Prandtl number, Pr, and characteristic length, L, and thermal conductivity λ. α is constant set equal to 0.07.

2.2. Evaporation Model

Liquid fuel is injected as a liquid column until breakup in the cylinder. The breakup time and initial SMD (Sauter Mean Diameter) are estimated according to Hiroyasu's correlations (Hiroyasu *et al.*, 1983). All droplets have the same initial diameter of the specified SMD and subsequently go through evaporation with decreasing droplet diameters. Liquid droplets obtain energy and go through evaporation through heat transfer from surrounding air. Heat transfer to droplets in the i-th spray zone is given as (Gosman and Johns, 1980)

$$q_i = C_{p_v}(T_g - T_{l,i})/(e^{z_i}-1)\frac{dm_{fg}}{dt} \tag{4}$$

so that $\dot{Q}_{fg} = \Sigma_{spray\ zones}\ q_i \cdot C_{p_v}$ is the specific heat of fuel vapor and z_i is the correction factor to consider the effects of boundary layer thickening. T_g is the temperature of surrounding air and $T_{l,i}$ is the temperature of liquid droplets given as (Borman and Johnson, 1962),

$$\frac{T_{l,i}}{dt} = \frac{1}{m_{l,i}C_{p_l}}\left(q_i - \lambda\frac{dm_{fg}}{dt}\right) \tag{5}$$

where $m_{l,i}$ is the mass of liquid fuel in each spray zone and C_{p_l} is the specific heat of liquid fuel. λ is latent heat of evaporation which is a function of temperature. $dm_{fg,i}/dt$ is the rate of evaporation given by

$$\frac{dm_{fg,i}}{dt} = \pi d_{l,i}N_i D_v Sh\frac{P}{R_v T_{m,i}}\ln\left(\frac{P}{P - P_{v,surf}}\right) \tag{6}$$

where $d_{l,i}$ is the mean diameter of droplets, D_v is diffusivity of fuel vapor, R_v is the gas constant, $T_{m,i}$ is mean temperature and $P_{v,surf}$ is the saturation pressure of fuel. N_i is the number of droplets in each zone determined by SMD, d_{32}, and mass of injected fuel, m_f, in each spray zone. The Sherwood number, Sh, is given from an experimental correlation (Jung, 2001).

2.3. Turbulent Burning Rate

The flame is assumed to propagate spherically with the burning rate given in terms of the mass remaining in a flame divided by the characteristic burning time as (Poulos, 1982),

$$\frac{dm_b}{dt} = \frac{m_e - m_b}{\tau} \tag{7}$$

where m_e and m_b are respectively entrained and burned mass in a flame brush. τ is the characteristic time to burn an eddy of the size, λ, and given by $\tau = \lambda/S_L$. The entrainment rate is given by $\dot{m}_e = \rho_u A_f V_e$ where A_f is the outer area for entrainment and V_e is the flame propagation speed. V_e is obtained by interpolation between S_L and S_T as,

$$V_e = \mathrm{K}S_T + (1-K)S_L \tag{8}$$

$$\text{with K} = \min\left[\left(\frac{\int S_L/l_t dt}{\alpha}\right)^n, 1\right]. \tag{9}$$

The flame moves initially at the laminar flame speed and later develops into a propagating turbulent flame. K becomes unity when the flame radius reaches α times the integral length scale, l_t, from the spark location. The exponent, n, determines the profile of kernel growth and is tuned to match the pressure trace for the reference case (Lee *et al.*, 2008). The laminar flame speed is calculated from an empirical correlation (Metghalchi and Keck, 1982) and turbulent burning velocity is given by Lee and Huh (2012)

$$S_T = AS_L\left(\frac{D_{tu}}{D_{mu}} + 1\right)^{1/2} \tag{10}$$

where A is a model constant and D_{mu} and D_{tu} are molecular and effective turbulent diffusivities.

2.4. Knock Model

As temperature and pressure increase, fuel is decomposed with heat release, although in a small amount at a low temperature in the unburned zone. Knock is assumed to occur when $Y_f^* = (Y_{f,u}^0 - Y_{f,u})/Y_{f,u}^0$, is equal to unity or at the time of rapid heat release with fuel consumption in the unburned zone. The reaction rate is described by the surrogate mechanism for mixtures of iso-octane and n-heptane with relative fractions according to the RON (Research Octane Number). The combined mechanism composed of 58 species and 214 steps is collected from the MultiChem mechanism (Ra and Reitz, 2011) for iso-octane and n-heptane including NOx.

The heat release from decomposition and knock, $\dot{Q}_{chem}$ is expressed as

$$\frac{dQ_{chem}}{dt} = \sum_i h_{f_i}\frac{dm_{i,u}}{dt} \tag{11}$$

where h_{f_i} is enthalpy of formation and $dm_{i,u}/dt$ is the rate of variation of the mass of the i-th species in the unburned zone. h_{f_i} and $dm_{i,u}/dt$ are calculated by the coupled CHEMKIN library.

An empirical knock model developed at IFP (Richard *et al.*, 2009) is employed for comparison with the predictions by skeletal chemistry of the surrogate mechanism for iso-octane and n-heptane in this work. The knock precursor, P, is computed as a function of the ignition delay and described by its mass fraction, Y_p, as

$$\frac{dY_p}{dt} = Y_{fuel}^0\frac{[\alpha^2\theta^2 + 4(1-\alpha\theta)(Y_p/Y_{fuel}^0)]^{1/2}}{\theta} \tag{12}$$

where Y_{fuel}^0 is the initial fuel mass fraction in the cylinder charge and $\alpha = 1.0\ s$ is a constant. θ is the ignition delay which is estimated by a simple AnB expression (Richard *et al.*, 2009). This formulation accounts for the conditions of unburned zone such as equivalence ratio, temperature, pressure and RON of fuel, but includes arbitrary modeling constants, A, n and B. Knock is assumed to occur, when the dimensionless knock delay, $\theta^* = Y_{fuel}^0/Y_p$, is equal to unity.

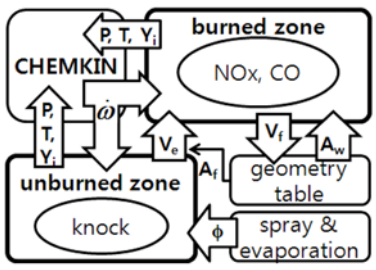

Figure 1. Structure of the quasi-dimensional code.

Refer to Richard *et al.* (2009) for further details on the empirical knock model.

3. STRUCTURE OF THE QUASI-DIMENSIONAL CODE

Figure 1 shows the computational flow through a four stroke cycle interacting with the CHEMKIN routine and the preprocessed geometry table. Mass flows between cylinder and intake/exhaust ports are calculated according to valve lift, pressure ratio and geometrical information including valve diameter, seat angle and port diameter. The combustion model requires flame area to calculate the rate of entrainment of unburned gas in the flame and wetted wall areas of burned and unburned gas for heat transfer on the wall. They are given from the geometry table obtained by preprocessing the engine mesh in advance. The CHEMKIN routine is coupled to calculate elementary reaction rates and update the species mass fractions in each zone under the pressure and temperature given from the main program. NOx and CO are computed in each burned zone and summed up for the total amount of emissions in the cylinder. Chemical reaction is also integrated to predict knock in the unburned zone.

4. SPECIFICATION OF THE TEST ENGINE AND ITS OPERATING CONDITIONS

Table 1 lists specifications of the test GDI engine and Figure 2 shows its operating conditions. We validated modified quasi-dimensional model for over 121 simulation points of the engine map in Figure 2. BMEP's are normalized by their maximum value due to restriction on release of specific engine data. The model constant A in Equation (10) is tuned to match calculated results with data fat 21 reference points (×symbols in Figure 2 over a wide range of engine speed and load conditions. Figure 3 shows the model constant, A, tuned for the 21 reference cases.

Table 1. Specifications of the test engine.

Displacement volume	590 cm^3
Bore	88 mm
Stroke	97 mm
Number of injection holes	6

Note that it tends to increase with speed and decrease with load. A is determined through interpolation of Figure 3 for the other 100 cases in Figure 2.

5. RESULTS AND DISCUSSION

Figure 4 shows measured and calculated pressure traces for the reference cases of the test engine in Figure 2. Results

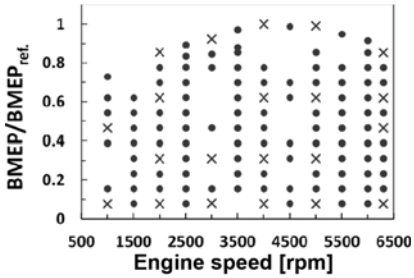

Figure 2. Operating conditions of the test engine (symbol ×represents the reference cases).

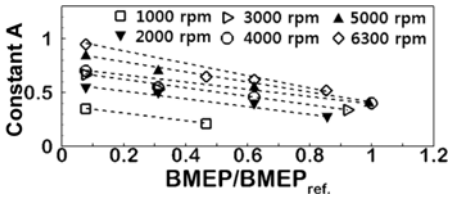

Figure 3. Model constant, A, tuned for 21 reference cases.

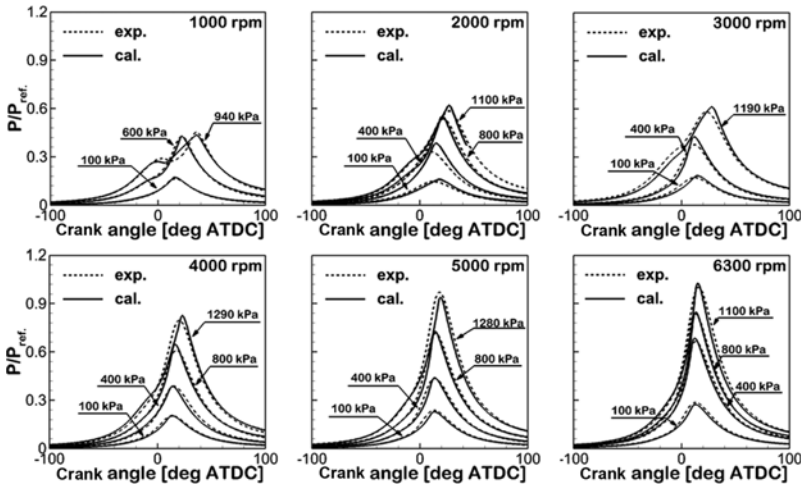

Figure 4. Measured and calculated pressure traces for 21 reference cases.

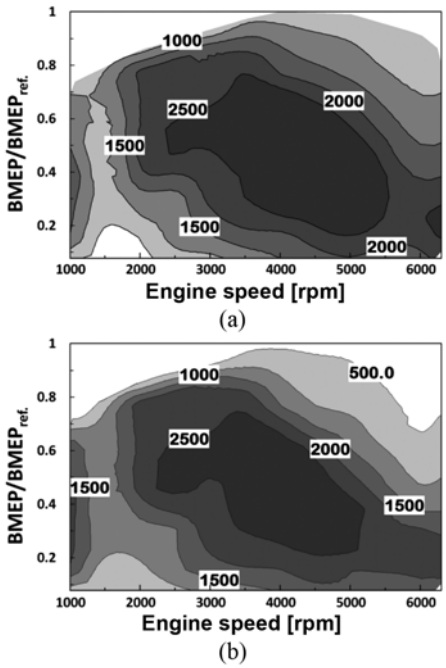

Figure 5. NOx concentrations (ppm) from (a) Measurement and (b) Calculation.

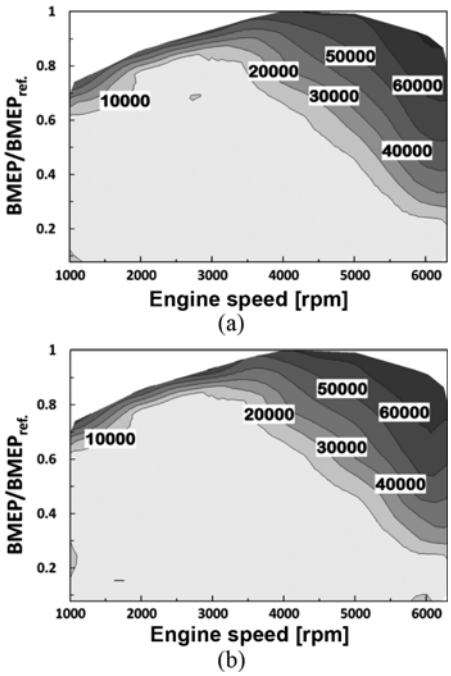

Figure 6. CO concentrations (ppm) from (a) Measurement and (b) Calculation.

are normalized by the measured peak pressure of the reference case at 6300 rpm and 1100 kPa BMEP due to restrictions on specific engine data. Note good agreement at different loads and rpms in Figure 4. The peak pressures and their timings are influenced primarily by the flame propagation speed, which is adjusted through two constants, α and n, in Equation (9). The peak pressure timing is retarded for a larger α, which determines transition from laminar to turbulent flame propagation. The constant n determines the profile of kernel growth to affect the slope of pressure increase. α is set equal to 0.06 and n is equal to 2 for all cases in this study.

Figure 5 shows measured and calculated NOx at all 121 points on the engine map in Figure 2. Note reasonable agreement of NOx emissions in the whole range of engine speed and load conditions. NOx increases due to higher peak pressure and temperature, as the load increases. There is an opposite trend for loads larger than about 0.62 BMEP/BMEP$_{ref.}$ with compositions richer than stoichiometric. Higher load cases show higher peak pressures in Figure 4, but lower NOx due to deficient oxygen in rich conditions in Figure 5. Both measured and predicted NOx tend to increase with the engine speed up to about 4000 rpm and to decrease again at higher rpms. Figure 6 shows measured and calculated CO with overall good agreement. The CO concentration does not show any consistent trend in stoichiometric conditions at loads below 0.62 BMEP/BMEP$_{ref.}$. The CO concentration increases with the equivalence ratio to show larger CO for higher load and rpm cases of richer compositions.

Figure 7 shows the cases of MBT timings and retarded spark timings to prevent knock and the calculated advanced spark timings when knock occurs. Results from the chemistry model are compared with those of the IFP model for the cases involving retarded spark timings in Figure 7 (a). Possibility of knock increases with the increasing peak pressure, as the spark timing is advanced in general. Both the chemistry and the IFP model predict knock under higher load and higher rpm conditions associated with higher peak pressures for the chemistry model in Figure 7 (b) and the IFP model in Figure 7 (c). Occurrence of knock is not predicted for all the cases including part load cases of retarded spark timings, while the two models show the same trends of knock for advanced spark timings.

It may be due to cyclic variation or local hot spots on the chamber wall such as an overheated valve or a spark plug, which are not taken into account in the quasi-dimensional model. It means that knock may occur by local effects rather than by increasing pressure or temperature of the cylinder charge in part load conditions.

Figure 8 shows the dimensionless knock delay, $\theta^* = Y^0_{fuel}/Y_p$ from the IFP model and $Y^*_f = (Y^0_{f,u} - Y_{f,u})/Y^0_{f,u}$ and the heat release rate from the chemistry model. Knock is assumed to occur when $\theta^*_f = 1$ or when $Y^*_f = 1$ in the unburned zone. More fuel decomposes with increasing possibility of knock for a lower RON, while there is minor heat release with no noticeable difference in the pressure trace. Figures 8 (a) and (c) at 1000 kPa and 1200 kPa BMEP show no knock for RON 92, as θ^* and Y^*_f do not reach unity and HRR in the unburned zone does not show any noticeable sharp peak. Knock occurs for RON 84 at the loads of 1000 kPa and 1200 kPa BMEP in Figures 8 (b) and 8 (d). Note

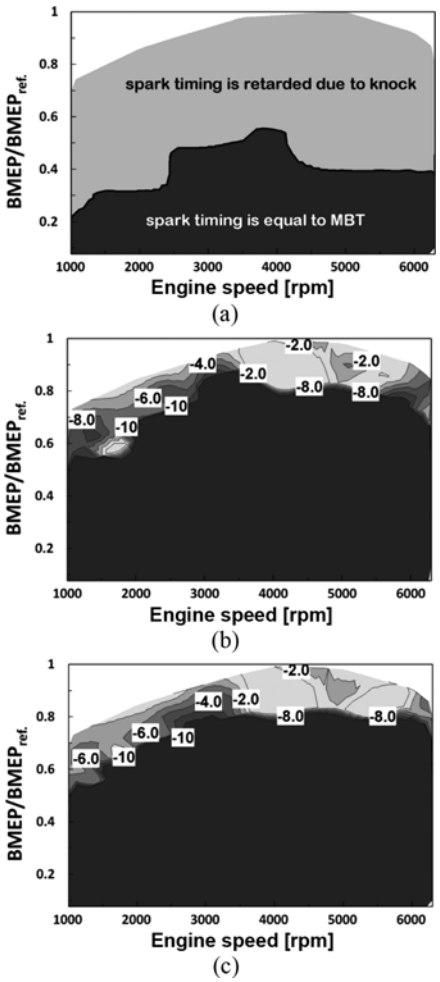

Figure 7. (a) Cases of MBT timings and retarded spark timings and calculated advanced spark timings [CA] when knock occurs by (b) Chemistry model and (c) IFP model.

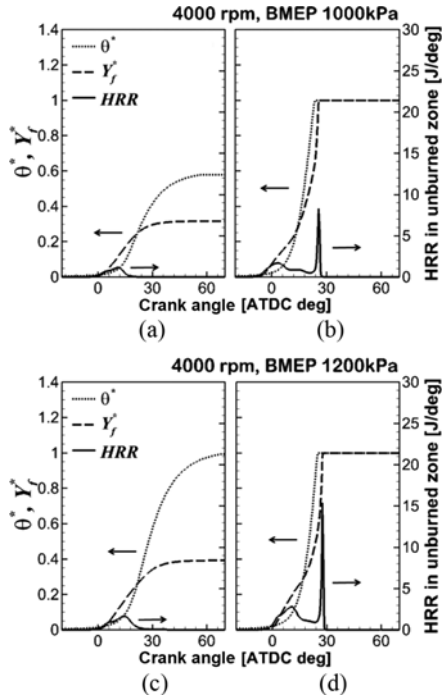

Figure 8. Variation of θ^*, Y_f^* and heat release rate (HRR) in the unburned zone at 4000 rpm: (a) 1000 kPa BMEP, RON 92; (b) 1000 kPa BMEP, RON 84; (c) 1200 kPa BMEP, RON 92 and (d) 1200 kPa BMEP, RON 84.

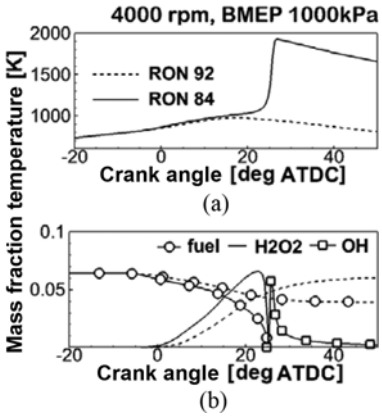

Figure 9. Comparison of (a) Temperature and (b) Species mass fractions in the unburned zone for RON 92 (dashed line) and RON 84 (solid line) fuels (H_2O_2 and OH fractions multiplied by 15 and 100 respectively).

rapid heat release and all fuel consumed in the unburned zone, once knock occurs. There is good agreement between the two knock models, while there is a little difference in the knock timings without tuning of model constants in this study.

Figure 9 shows temporal variation of temperature and relevant species concentrations for fuels of RON 92 and 84. Knock does not occur for RON 92, while RON 84 represents a knocking condition with rapid heat release in the temperature profile in Figure 9 (a). Difference lies in the rate of fuel decomposition to produce H_2O_2 by low temperature chemistry during the ignition delay period. H_2O_2 is consumed to form OH which again reacts to form H_2O with rapid heat release and increase in the unburned gas temperature, once knock occurs in Figure 9 (b). The temperature should exceed 900 K for chain branching steps to produce a large concentration of OH radicals as for RON 84. There is no such variation of temperature, H_2O_2 and OH concentrations in unburned gas until combustion is complete for RON 92.

6. CONCLUSION

(1) A quasi-dimensional code is developed for efficient calibration of a four stroke cycle homogeneous GDI engine. It includes models for spray, burning rate and chemistry for emissions and knock validated for the

test engine. It is combined with CHEMKIN routines to perform integration of elementary reaction steps together with multizone mass and energy conservation equations to consider temperature stratification in the main program.

(2) There is good agreement between measured and predicted pressure traces for different load and rpm conditions. The peak pressure and timing are primarily influenced by the flame propagation speed which is adjusted through two constants for transition of a growing flame kernel between laminar and turbulent propagation speed. The constants are tuned to match pressure traces of 21 reference cases and applied to all 121 cases in the engine map with interpolated constants.

(3) There is good agreement for NOx, which increases with load and rpm respectively due to higher peak temperature and reduced heat loss. Results shows lower NOx for mixture compositions richer than stoichiometric. CO does not show any consistent trend for the stoichiometric composition, while mixture richer than stoichiometric leads to lower NOx and higher CO. There is also good overall agreement between measured and calculated CO concentrations.

(4) Knock is modeled by the surrogate mechanism for mixture of n-heptane and isooctane. There is reasonable agreement with the empirical IFP knock model which involves arbitrary constants tuned for a specific engine. Parametric study is performed for fuels of different RON's with proper trends of variation by the chemistry model. It allows consistent prediction for different fuels, engine designs and operating conditions without any arbitrary tuning of model constants.

REFERENCES

Blizard, N. S. and Keck, J. C. (1974). Experimental and theoretical investigation of turbulent burning model for internal combustion engines. *SAE Paper No.* 740191.

Borman, G. L. and Johnson, J. H. (1962). Unsteady vaporization histories and trajectories of fuel drops injected into swirling. *SAE Paper No.* 620271.

Bougrine, S., Richard, S. and Veynante, D. (2011). On the combination of complex chemistry with a 0-D coherent flame model to account for the fuel properties in spark ignition engines simulations: Application to methane-air-diluents mixtures. *Proc. Combust. Inst*., **33**, 3123.

D'Errico, G. and Onorati, A. (2004). An integrated simulation model for the prediction of GDI engine cylinder emissions and exhaust after-treatment system performance. *SAE Paper No.* 2004-01-0043.

Gong, J. and Rutland, C. (2013). A quasi-dimensional NOx emission model for spark-ignition direct injection (SIDI) gasoline engines. *SAE Paper No.* 2013-01-1311.

Gosman, A. D. and Johns, R. J. R. (1980). Computer analysis of fuel-air mixing in direct-injection engines. *SAE Paper No.* 800091.

Grill, M., Billinger, T. and Bargende, M. (2006). Quasi-dimensional modeling of spark ignition engine combustion with variable valve train. *SAE Paper No.* 2006-01-1107.

Han, S. (1997). *Design and Demonstration of a Spark Ignition Engine Operating in a Stratified-EGR Mode*. Ph. D. Dissertation. MIT. Massachusetts.

Hiroyasu, H., Kadota, T. and Arai, M. (1983). Development and use of a spray combustion modeling to predict diesel engine efficiency and pollutant emissions (Part 1: Combustion Modeling). *JSME*, **26**, 569.

Jung, D. (2001). *A Multi-zone Direct-injection Diesel Spray Combustion Model for Cycle Simulation Studies of Large-bore Engine Performance and Emissions*. Ph. D. Dissertation. University of Michigan. Michigan.

Lee, D., Han, I., Huh, K. Y., Lee, J. H., Kim, S. J., Kang, W. and Kim, Y. (2008). A new combustion model based on transport of mean reaction progress variable in a spark ignition engine. *SAE Paper No.* 2008-01-0964.

Lee, D. and Huh, K. Y. (2012). Validation of analytical expression for turbulent burning velocity in stagnating and freely propagating turbulent premixed flames. *Combust. Flame*, **159**, 1576.

Malbec, L. M., Le Berr, F., Richard, S., Font, G. and Albercht, A. (2009). Modelling turbocharged spark-ignition engines: Towards predictive real time simulators. *SAE Paper No.* 2009-01-0675.

Metghalchi, M. and Keck, J. C. (1982). Burning velocity of mixtures of air with methanol, isooctane, and indolene at high pressure and temperature. *Combust. Flame*, **48**, 191.

Poulos, S. G. (1982). *The Effect of Chamber Geometry on SI Engine Combustion Rates-A Modeling Study*. M. S. Thesis. MIT. Massachusetts.

Ra, Y. and Reitz, R. D. (2011). A combustion model for IC engine combustion simulations with multi-component fuels. *Combust. Flame*, **158**, 69.

Richard, S., Bougrine, S., Font, G., Lafossas, F.-A. and Le Berr, F. (2009). On reduction of a 3D CFD combustion model to build a physical 0D model for simulating heat release, knock and pollutants in SI engines. *Oli Gas Sci. Technol.* **64**, 223.

Schmid, A., Grill, M., Berner, H. J., Bargende, M., Rossa, S. and Böttcher, M. (2009). Development of a quasi-dimensional combustion model for stratified SI-engine. *SAE Paper No.* 2009-01-2659.

Tabaczynski, R. J., Ferguson, C. R. and Radhakrishnan, K. (1977). A turbulent entrainment model for spark-ignition engine combustion. *SAE Paper No.* 770647.

Tinaut, F. V., Melgar, A. and Horrillo, A. (1999). Utilization of a quasi-dimensional model for predicting pollutant emissions in SI engines. *SAE Paper No.* 1999-01-0223.

Watanabe, K., Ito, S. and Tsurushima, T. (2010). A new quasi-dimensional combustion model applicable to direct injection gasoline engine. *SAE Paper No.* 2010-01-0544.